HOSTED BY
ELSEVIER
Available online at www.sciencedirect.com
ScienceDirect
Soils and Foundations 61 (2021) 642–657
www.elsevier.com/locate/sandf

Technical Paper

Investigation of soil deformation characteristics during pullout of a ribbed reinforcement using X-ray micro CT

Ryunosuke Kido [a,*], Yasuo Sawamura [b], Koshi Kimura [c], Makoto Kimura [a]

[a] Department of Civil and Earth Resources Engineering, Kyoto University, Japan
[b] Department of Urban Management, Kyoto University, Japan
[c] Ministry of Economy, Trade and Industry, Japan

Received 30 July 2020; received in revised form 22 January 2021; accepted 28 January 2021
Available online 26 March 2021

Abstract

Steel-strip reinforced earth walls stabilize through the pullout resistance of the reinforcements. Soil dilation during the pullout of ribbed reinforcements may contribute to the evolution of pullout resistance; however, few studies have clarified this mechanism by investigating how soils behave with increasing pullout displacement. The ribs of the reinforcements enhance the pullout resistance, although the influence of the rib dimensions on the evolution of pullout resistance with increasing pullout displacement has not been sufficiently revealed. In the present study, a triaxial pullout apparatus is developed and pullout tests are conducted using ribbed reinforcements with different rib-inclination angles under isotropic stress. The displacement and strain fields in the soils during the pullout of the reinforcements are investigated by X-ray micro CT and a digital image correlation technique. It is found that larger rib-inclination angles provide higher pullout resistance at an early stage of the pullout because of the higher bearing resistance related to the more significant soil densification above the ribs. With increasing pullout displacement, the reinforcements with different rib-inclination angles come to behave as almost one in the same since a rigid soil wedge related to the passive soil failure is generated above the ribs. This tendency results in similar soil deformation characteristics and pullout resistance levels for every reinforcement beyond the soil failure state, although the rib-inclination angles are different.

Keywords: Pullout test; Ribbed reinforcement; Rib-inclination angle; Pullout resistance; X-ray micro CT

1. Introduction

The use of steel-strip reinforced earth walls (SSREWs) represents one of the reinforced earth wall methods, comprising ribbed steel reinforcements and rigid walls. Since these structures were first adopted for road embankments by France in 1964, their use has become widespread all over the world (e.g., Hirai et al., 2003; James and Willem, 1987; Jones, 1985). The seismic performance of SSREWs has been investigated by conducting seismic full-scale model tests (Richardson and Lee, 1975; Richardson et al., 1977) and centrifuge model tests (Siddharthan et al., 2004; Sawamura et al., 2019). It was reported in post-earthquake investigations (e.g., Kuwano et al., 2014; Miyata, 2014; Sawamatsu et al., 2018) that most SSREWs experienced no damage or only slight damage, although many infrastructures were severely damaged. It can be said, therefore, that SSREWs exhibit a high seismic performance.

The stability of SSREWs is provided by the frictional resistance between the ground and the reinforcements. In the current Japanese design guidelines for internal stability,

Peer review under responsibility of The Japanese Geotechnical Society.
* Corresponding author.
E-mail address: kido.ryunosuke.2m@kyoto-u.ac.jp (R. Kido).

https://doi.org/10.1016/j.sandf.2021.01.013
0038-0806/

the reinforced length and laying interval of the strips are determined by the limit equilibrium method, considering the maximum pullout resistance (Public Works Research Center, 2014). On the other hand, reinforced earth walls, representative of SSREWs, are typically flexible compared to other infrastructures. Namely, their deformation is relatively allowed and then the pullout resistance of the reinforcements is exhibited. According to the Public Works Research Center (2014), levels of wall displacement that are less than 0.3 m, or less than 3% of the wall height, are determined as the design criterion whereby reinforced earth walls are stable. It is important, therefore, to consider the performance of the individual reinforcements during deformation when evaluating the stability of the structures.

In previous studies, the evolution of the pullout resistance of reinforcements was measured by pullout tests (e.g., Jayawickrama et al., 2015; Li et al., 2017; Rahmaninezhad et al., 2016; Schlosser and Elias, 1978; Weldu et al., 2016). Schlosser (1982) suggested that the restraint of soil dilation around reinforcements by the surrounding soils enhances the confining pressure acting on the reinforcements, resulting in higher pullout resistance. However, few studies have confirmed how soils behave during the pullout of reinforcements and then how they affect the evolution of pullout resistance. The pullout resistance is generated by soil-reinforcement interactions; and hence, laboratory tests to visualize the soil behavior around the reinforcements contribute to the clarification of the mechanism of the pullout resistance evolution.

It was also found that ribbed reinforcements exhibit higher pullout resistance than flat strips (e.g., Schlosser and Elias, 1978; Ogawa, 1997); this trend is quite similar to the results whereby belled piles show higher uplift resistance than straight piles (e.g., Moayedi and Mosallanezhad, 2017). Namely, the pullout resistance of ribbed reinforcements probably depends not only on the friction between the soils and the reinforcements, but also the bearing resistance at the ribs. With respect to the rib dimensions, typical values for the rib height and the rib-inclination angle are described in the guidelines of the Public Works Research Center (2014) and Ogawa (1997), respectively. However, these values have been empirically used without sufficient verification. Investigating the influence of the rib dimensions on the pullout resistance evolution of the reinforcements will confirm the conventional design for ribbed reinforcements or aid in the development of a better design for them.

An X-ray CT technique is one of the most effective tools for observing geomaterial behavior (e.g., Desrues et al., 1996; Otani et al., 2000). Grain kinematics (e.g., Andò et al., 2012; Druckrey et al., 2018), the strain localization of a partially saturated sand (e.g., Higo et al., 2011; Kido and Higo, 2019), and pore structures and pore fluids (e.g., Hamamoto et al., 2016; Higo et al., 2018; Mukunoki et al., 2016; Kido et al., 2020) have been investigated using X-ray micro CT. Soil-structure interaction, in structures such as pile foundations, has also been investigated by the X-ray CT. Otani (2003) investigated the change in soil density during a pile penetration under one-dimensional confining pressure by a dead load. It seems difficult, however, to represent the field condition (i.e., K_0-stress condition) because the applicable level of confining pressure by the dead load was lower than 20 kPa. Doreau-Malioche et al. (2018) developed a triaxial apparatus for a pile penetration test with X-ray CT that provides isotropic confining pressure higher than 100 kPa, which makes it possible to demonstrate the stress condition closer to that of the field ground compared with the one-dimensional confining pressure. On the other hand, few studies have investigated the soil deformation characteristics during the pullout of a reinforcement using X-ray CT under any level of confining pressure.

The present study develops a triaxial pullout apparatus to perform pullout tests on a ribbed reinforcement with X-ray micro CT under any level of isotropic confining pressure, demonstrating a reinforcement placed in a reinforced earth wall (Fig. 1). Pullout tests are conducted with four kinds of ribbed reinforcements having different degrees of rib-inclination angles and two rib heights, through which the influence of the rib dimensions on the pullout resistance is examined. CT images focusing on the soils around the rib are obtained at different pullout displacement levels, and then the displacement and the strain fields are quantified. The soil deformation characteristics during the pullout of

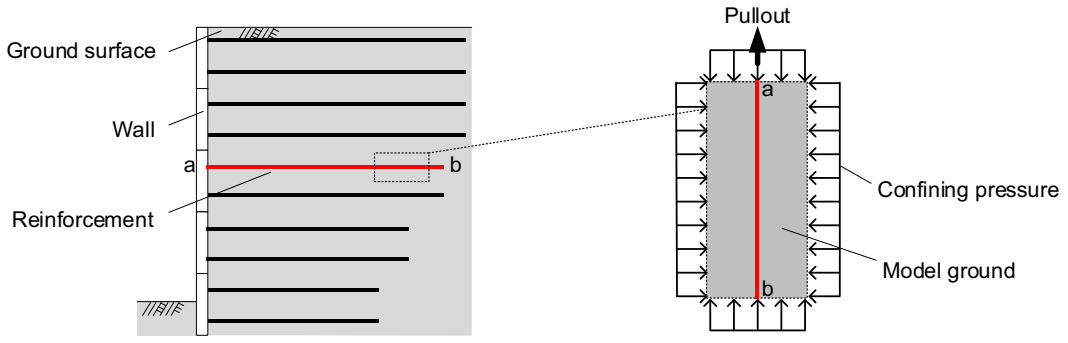

Fig. 1. Demonstration of reinforcement placed in reinforced earth wall.

the ribbed reinforcements and their influence on the evolution of pullout resistance are discussed.

2. Experimental methods

2.1. Triaxial pullout apparatus

Fig. 2a shows a schematic illustration of the triaxial pullout apparatus developed in the present study. This apparatus comprises a triaxial cell and a base plate. The cell is made of lucid acrylic, 10 mm in thickness, 120 mm in internal diameter and 2 MPa in pressure resistance, in order to avoid x-ray attenuation as much as possible and to support the axial load without steel pillars (e.g., Higo et al., 2011; Kikuchi, 2006; Otani et al., 2002). A motor is equipped on the cell to adjust the pullout rate of the reinforcements to be between 0.1 mm/min and 1.0 mm/min, and the models are manually moved by a handle. A contact-type displacement gauge and a load cell measure the displacement and the pullout resistance, respectively. The cell pressure and the inner pressure of the model grounds are measured by two pressure gauges, respectively. The load cell is connected to a steel bar, 20 mm in diameter and 200 mm in length, and each reinforcement is fixed to the steel bar using a pin. An acrylic pedestal, 69 mm in diameter and 40 mm in height, is placed on the base plate. The tip of each reinforcement can be inserted into a hollow on the pedestal, by which the model is placed vertically during the preparation of the ground. Two porous stones, 20 mm in diameter and 5 mm in thickness, are embedded in the pedestal, thorough which the inner ground is exposed to atmospheric pressure.

2.2. X-ray micro CT

The X-ray micro CT facility used in the present study is KYOTO-GEOμXCT (Kido et al., 2020), which was assembled by TOSHIBA IT and Control Systems Corporation and installed in the Department of Civil and Earth Resources Engineering of Kyoto University. Fig. 2b presents a photo of the testing system. The spot size of the X-ray source and the resolution performance are 4 μm and 5 μm, respectively. The voltage and the current are independently controlled within a maximum consumption power of 200 W. The work table is moved upwards and downwards, to the left and to the right, and rotated 360 degrees. The X-ray attenuation into a specimen on the table is recorded by the detector and then CT images are reconstructed. A cone-beam scan provides several slices in the vertical direction at the same time, namely, a three-dimensional tomographic volume can be obtained. Each slice of the CT images obtained in the present study is composed of 1024^2 voxels. Each voxel shows a CT value determined by converting the X-ray absorption coefficients, which depend on the material densities. Desrues et al. (1996) and Higo et al. (2011) confirmed that there is an almost linear relationship between the material density and the X-ray absorption coefficient, i.e., the CT value.

2.3. Reinforcements

The reinforcements used for reinforced earth walls have several ribs on both faces at certain intervals. In the present study, acrylic round bars with disk-shaped ribs were prepared as the reinforcement. The main reasons are 1) to avoid the inconvenience of image processing due to a metal artifact of CT images scanning metal inclusions, 2) to capture the soil behavior during the pullout of the reinforcement under a symmetric condition for the soil deformation and 3) to discuss the influence of ribs on the relationship between the soil deformation and the pullout resistance. The physical properties of the acrylic include a Young's modulus of 1.19 GPa and tensile strength of 65 MPa.

Fig. 3 presents a schematic illustration of the reinforcements. As shown in Fig. 3a, the typical dimensions of a

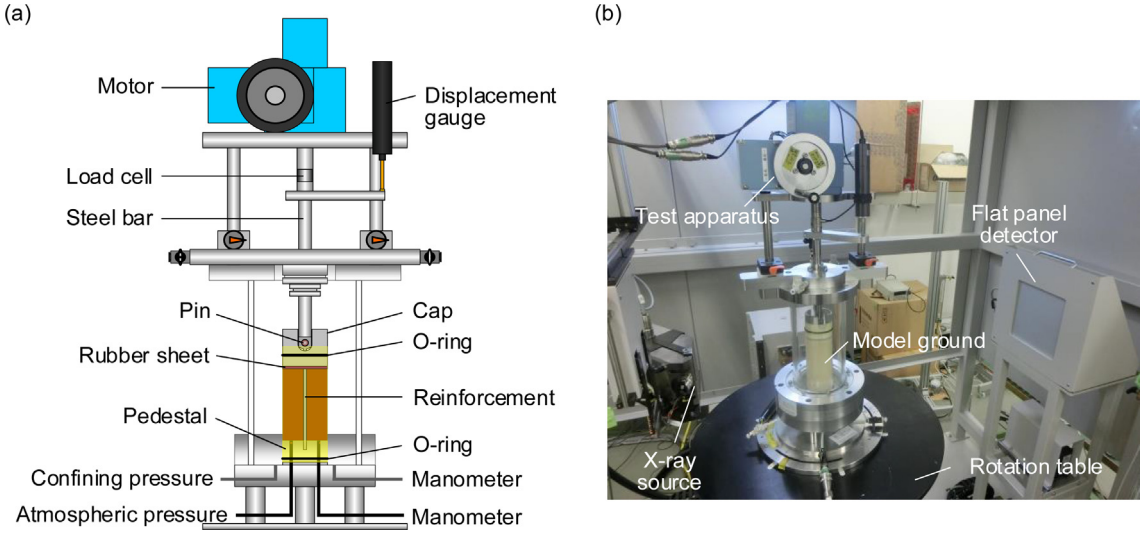

Fig. 2. (a) Schematic illustration of triaxial pullout apparatus and (b) photo of testing system.

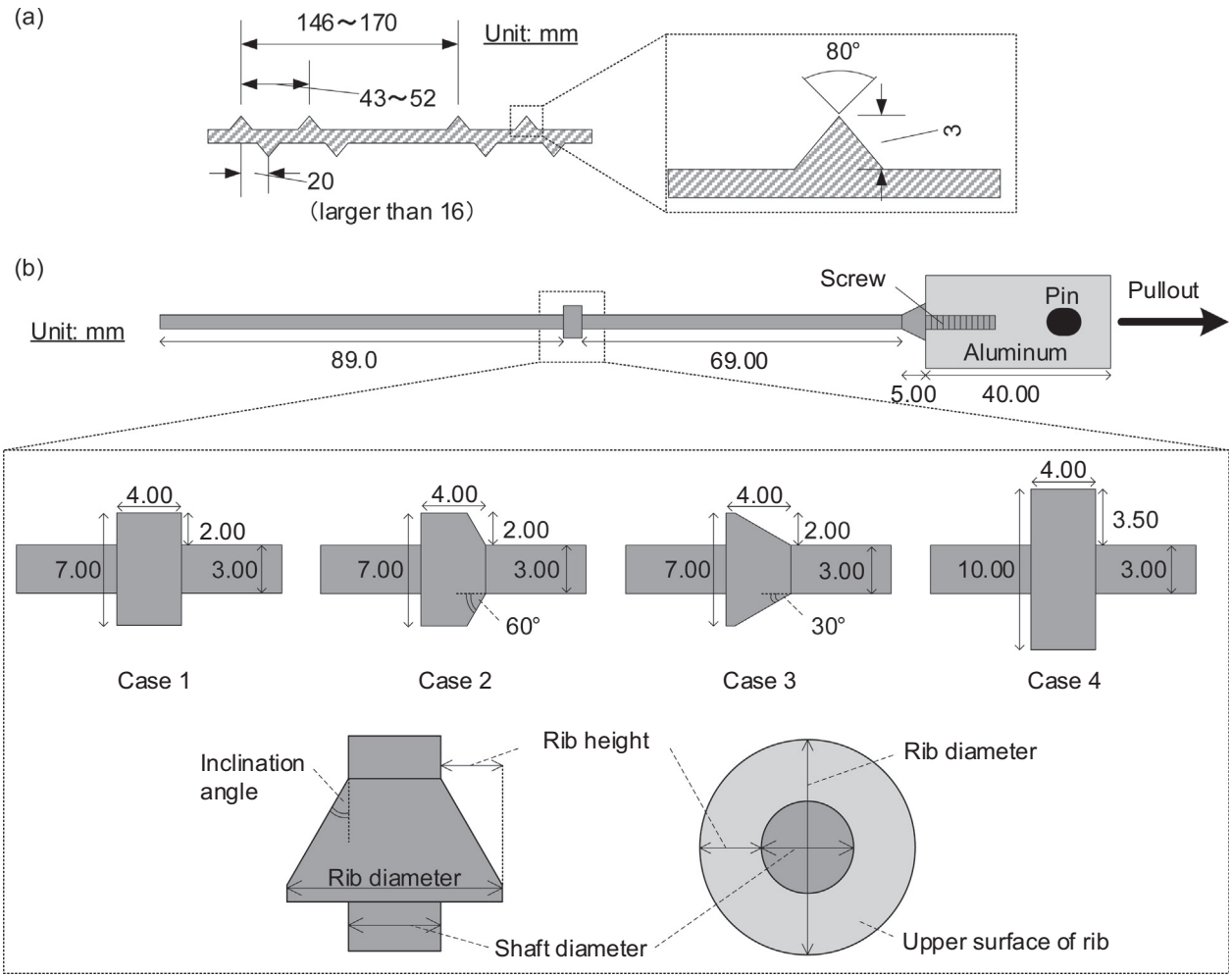

Fig. 3. (a) Schematic illustration of real ribbed reinforcement and (b) four kinds of ribbed reinforcements.

ribbed reinforcement used for steel-strip reinforced earth walls include a rib height of 3 mm (Public Works Research Center, 2014) and a rib-inclination angle of 50 degrees (Ogawa, 1997). The objective of the present study is to investigate the influence of the rib-inclination angle on the pullout resistance. Therefore, three reinforcements with different inclination angles are prepared, as shown in Fig. 3b: 90 degrees for Case 1 (flat rib), 60 degrees for Case 2 and 30 degrees for Case 3. The rib height of these models is 2 mm. Another reinforcement, with an inclination angle of 90 degrees and a rib height of 3.5 mm, is also prepared as Case 4 in order to investigate the influence of the rib height on the pullout resistance. The shaft diameter for all the reinforcements is 3 mm.

2.4. Model ground

The sample used in the present study is Toyoura sand; Table 1 lists the physical properties of this sand. The diameter and the height of the model ground are 69 mm and 140 mm, respectively. The reinforcement is placed at the center of the model ground. When isotropic confining pressure is applied to the model ground, for example, in triaxial tests, the cell pressure should be applied to the model ground while exposing the inner ground to atmospheric pressure through a model cap. On the other hand, the reinforcement should be out of the upper part of the model ground during the pullout test. It is difficult, therefore, to apply cell pressure in the pullout tests while exposing the ground to atmospheric pressure using a model cap. In the present study, the isotropic pressure condition was accomplished using three membrane sheets, 0.2 mm in thickness, and a rubber sheet, 3 mm in thickness.

Fig. 4 presents the procedure for preparing the model ground. A membrane, 0.3 mm in thickness, was fixed to

Table 1
Physical properties of Toyoura sand.

Particle density [g/cm^3]	2.64
Maximum void ratio	0.975
Minimum void ratio	0.585
D_{50} [mm]	0.200
ϕ^{p} [°] (peak stress)	38.9
ϕ^{r} [°] (residual stress)	33.4
$\phi^{r(T\text{-}a)}$ [°] (between Toyoura sand and acryl)	20.3

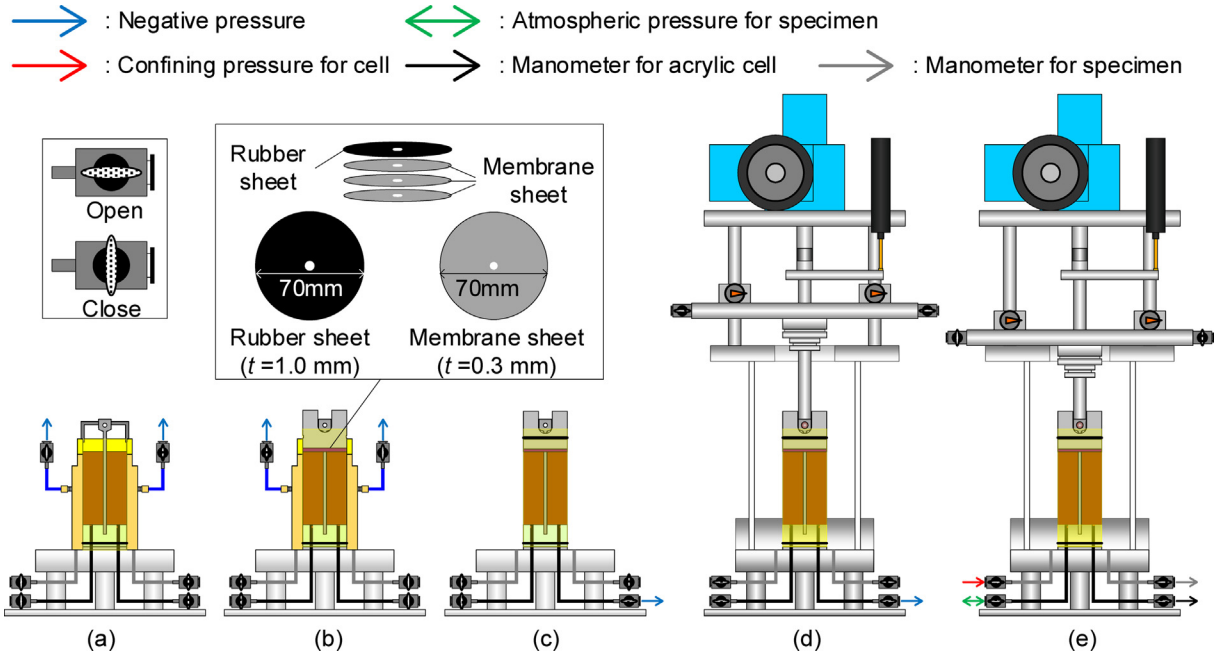

Fig. 4. Procedure for preparing specimen: (a) pouring sand, (b) setting rubber sheet and cap, (c) applying negative pressure to specimen, (d) connecting by pin and (e) applying confining pressure to cell.

the pedestal using an O ring. A mold was attached to the pedestal and then the membrane was stuck to the inner mold by applying a negative pressure of 40 kPa. The tip of the reinforcement, to which the three membrane sheets were attached beforehand, was inserted into a hollow on the pedestal, and the upper part of the model was fixed by a jig placed on top of the mold. Then, air-dried Toyoura sand was poured and compacted in 10 layers to prepare the model ground with a height of 140 mm, and the relative density (D_r) was 90%.

Once the model ground had been prepared, the three membrane sheets were placed on the surface of the ground and then a rubber sheet was put on them (Fig. 4b). An aluminum cap was replaced with the jig on the top of the mold. The negative pressure applied to the mold was removed and then negative pressure was applied to the inner ground, by which the ground can stand by itself (Fig. 4c). The steel bar, the load cell and the reinforcement were connected, after which the triaxial cell was fixed to the base plate using screws (Fig. 4d). Finally, the negative pressure applied to the inner ground was released and then a prescribed amount of cell pressure was applied by air pressure as the confining pressure (Fig. 4e).

2.5. Pullout test conditions

Previous researchers have performed pullout tests on reinforcements under a pullout rate equal to or greater than 1.0 mm/min (e.g., Lawson et al., 2013; Lee and Bobet, 2005; Rathje et al., 2006). In the present study, the pullout tests were performed with a pullout rate of 0.5 mm/min because of the convenience of adjusting the displacement where X-ray tomography was performed. The displacement of 7 mm, which is consistent with the 5% length of the reinforcement embedded in the ground, was applied. The pullout resistance and displacement were measured every second during each test. Three pullout tests were performed for each case without X-ray tomography.

Isotropic confining pressure of 100 kPa was applied to the model ground. In the present study, the difference between the cell pressure and the inner ground pressure is assumed as the confining pressure. Fig. 5 shows an example of the confining pressure measured during the pullout test, in which the cell pressure of 100 kPa was applied. It is clearly seen that the inner ground pressure is kept at almost atmospheric pressure while applying the cell pressure. The confining pressure level is similar to the vertical stress level at the deeper part of the backfill where the height falls in

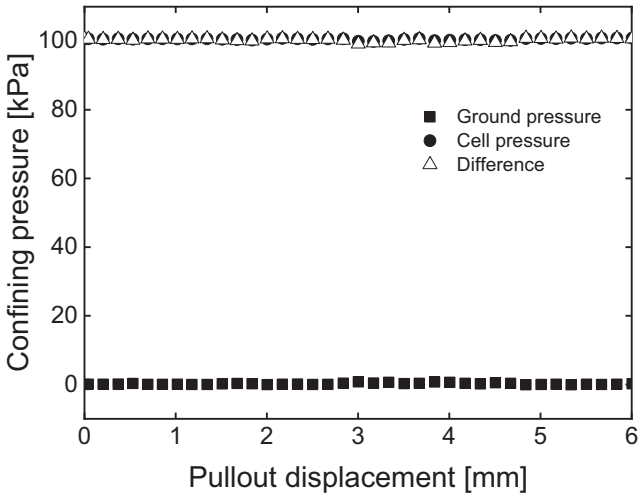

Fig. 5. Confining pressure-pullout displacement relationship.

the range of 5 m to 8 m, assuming the typical wall heights of SSREWs. Under high levels of confining pressure, particle breakage is one of the concerns affecting the pullout behavior of the reinforcements, whereas the Toyoura sand exhibits almost no particle breakage during shearing under hundreds of kPa (Miura and Yamauchi, 1977).

2.6. Differences in test conditions from field conditions

2.6.1. Model ground scale

Lee and Bobet (2005), for example, used a soil chamber whose dimensions are 1.0 m long, 0.4 m wide and 0.5 m high, and a steel strip whose dimensions are identical to the commercial strips: 0.75 m long embedded into the soil, 5 cm wide and 3 mm thick. Similarly, such a set of equipment has been designed and applied in other large-scale pullout tests (e.g., Weldu et al., 2016; Rahmaninezhad et al., 2016), which can simulate the field behavior of the reinforcement. Both the model ground and the reinforcement used in the present study are much smaller than those used in the previous pullout tests. Therefore, it is difficult to completely demonstrate the pullout behavior of the reinforcement under the field condition.

The main purpose of the present study is to observe how soils behave around ribbed reinforcements using the X-ray CT technique. In order not only to achieve a sufficient amount of X-ray attenuation to obtain high resolution images, but also to reduce the negative influence of the model ground scale on the soil behavior, as much as possible, the dimensions of the model ground are designed considering the limitations of the overall weight on the X-ray table.

2.6.2. Boundary conditions

The lateral sides of the model ground used in the present study are in a flexible condition due to the membrane. Thus, soil movement may be allowed compared to a fixed condition. Considering the above-mentioned ratio, it is possible that the soil deformation reaches the membrane boundary if the rib height is relatively large. In this case, the restraint degrees of soil dilation by the surrounding soils during the pullout of reinforcements is varied, affecting the evolution of pullout resistance. On the other hand, the present study confirms with X-ray CT that the soil deformation occurs within the scan area. The membrane boundary is 20 mm from the scan area, namely, the soil deformation around the boundary is quite small. Therefore, the influence of the membrane boundary on the pullout behavior is not significant in spite of having a different boundary from that of the field conditions.

The top of the model grounds used in the present study is supported by a cap. This cap is connected to the membrane via an O ring; and thus, the cap may move upwards with the soil movement during the pullout of a reinforcement. In this case, the overall model ground is lifted up, which makes evaluating soil-reinforcement interactions impossible. It has been confirmed, however, that such a phenomenon is not observed here and that the soil deformation does not reach the cap with the pullout displacement levels given in the present study (7 mm). Therefore, the influence of the top cap on the pullout behavior is not significant.

2.6.3. Setup and pullout directions of reinforcements

The reinforcement used in the present study is vertically placed in the model ground, which is different from the field conditions, as shown in Fig. 1. In other words, the force of gravity is applied to the axial direction of the model ground and the reinforcement. In this case, the force of gravity may influence the degrees of soil movement and the model ground may be unstable when applying insufficient levels of isotropic confining pressure. To avoid both situations, as much as possible, the relatively higher but realistic confining pressure of 100 kPa was applied, as mentioned in Section 2.5.

3. Results and discussions

3.1. Pullout tests of reinforcement

Fig. 6 shows the pullout resistance-pullout displacement relationship and the resistant gradient-displacement relationships up to 6 mm for the displacement where the pullout resistance almost converges. As shown in Fig. 6f, the resistant gradient is defined as a ratio of the difference in the pullout resistance to that in the pullout displacement measured in one second. The displacement where the resistant gradient reaches zero is defined as a failure point, and the pullout resistance at a failure point is defined as the ultimate resistance. Table 2 lists the average values of the failure points and the ultimate pullout resistance obtained by three tests for each case. In the pullout tests with CT, stress relaxations occur since the displacement is kept constant due to the suspension of the pullout of the reinforcement during the CT scan. Fig. 6a to d indicate that, for all cases, the levels of pullout resistance obtained by the three tests without CT are almost similar to each other and the pullout resistance obtained in the test with CT is similar to that obtained in the test without CT. In other words, the influence of the stress relaxation during the CT scan on the pullout resistance is small.

Fig. 6e presents a comparison of the pullout resistance for all cases, in which the results obtained in each test without CT, closest to those with CT, are shown as the representative values. It is found from Fig. 6e and Table 2 that Case 4 shows higher resistance than the other cases. Comparing the results among Cases 1, 2 and 3, the pullout resistance for Case 1 is higher than the resistance for either Case 2 or Case 3 at an early stage of the pullout, while the levels of pullout resistance for the three cases are similar to each other with an increase in the displacement. These results indicate that the pullout resistance depends on the rib height rather than the rib-inclination angle.

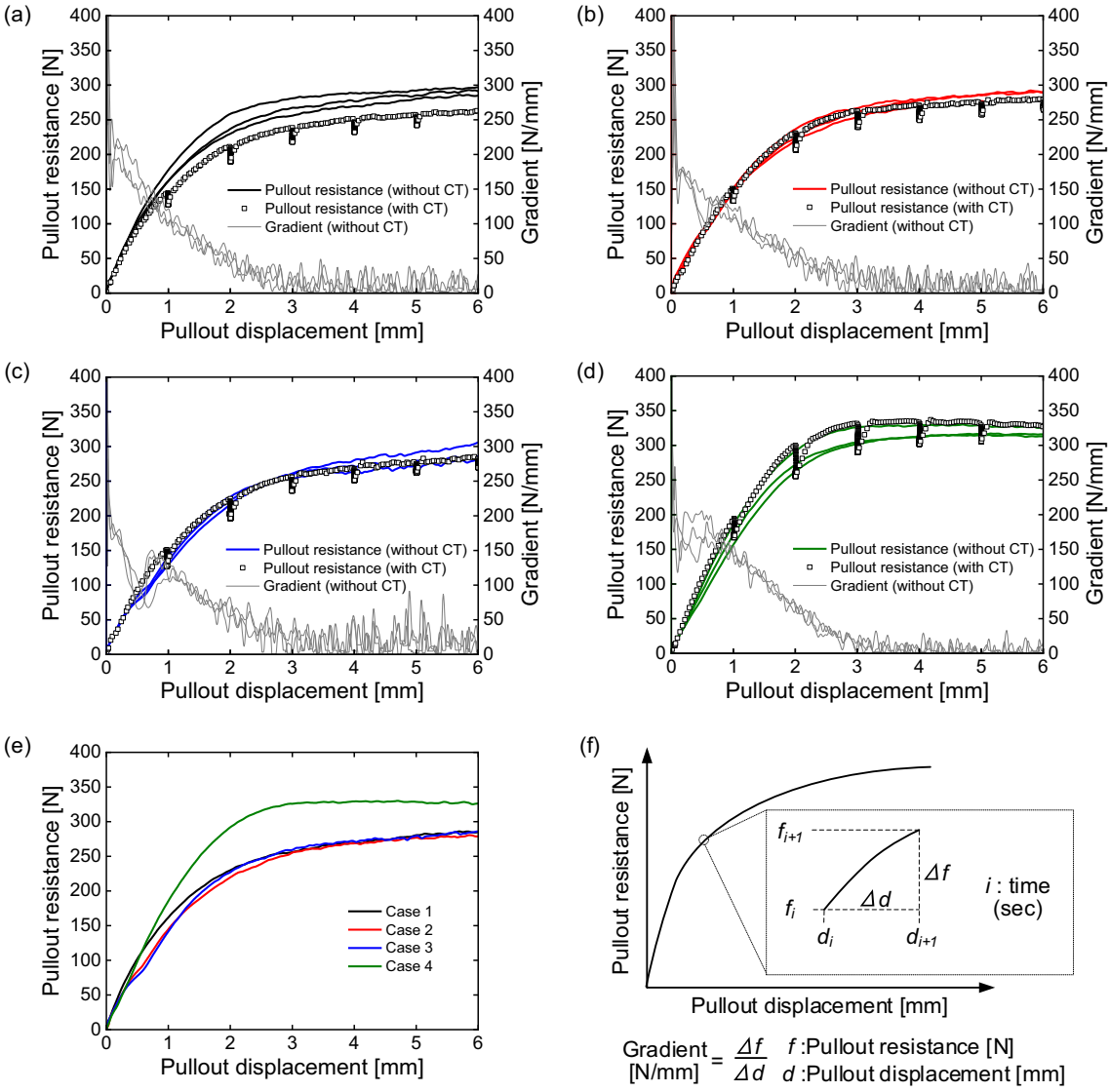

Fig. 6. Pullout resistance-pullout displacement relationships: (a) Case 1, (b) Case 2, (c) Case 3, (d) Case 4, (e) representative pullout resistance for all cases and (f) schematic diagram of calculation of gradient.

Table 2
Average failure point and average ultimate pullout resistance.

Case	1	2	3	4
Average failure point [mm]	2.86	3.25	2.95	3.26
Average ultimate pullout resistance [N]	267.64	266.26	256.21	314.59

The pullout resistance for Cases 1 to 3 tends to increase without a distinct peak value and that for Case 4 slightly decreases after the peak value, as shown in Fig. 6. Similar trends in the changes of the pullout resistance have been observed in previous studies (Lee and Bobet, 2005; Weldu et al., 2016; Rahmaninezhad et al., 2016), although the level of pullout resistance measured in the present study is quite a bit lower than that measured in them. Hence, the small-scale tests conducted in the present study qualitatively simulate the pullout behavior of the reinforcement placed into the soil. This makes it possible to discuss the relationship between the pullout resistance and the soil deformation.

3.2. X-ray CT images

The displacement levels for the CT scan are determined based on the failure point for each case. As shown in Table 2, the failure points for Cases 1 to 4 are almost 3 mm; and hence, a displacement of 3 mm is determined as the criterion for the CT scan. CT scans are performed from the initial state to the failure point every 1 mm:

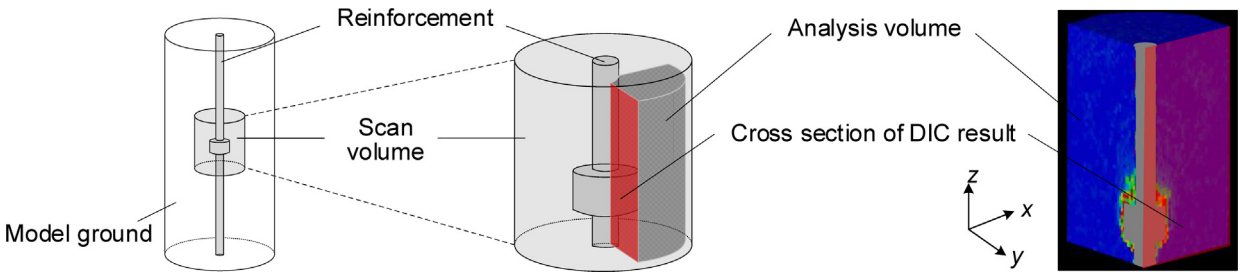

Fig. 7. Analysis volume out of scan volume.

0 mm, 1 mm, 2 mm and 3 mm. After that, CT scans are performed at displacements of 4 mm, 5 mm and 6 mm. Fig. 7 shows the scan area and an image processing area to be described later. In the present study, out of the whole model ground, a cylindrical region of interest, 30.80 mm in diameter and 30.40 mm in height, is observed at each stage of the pullout of the reinforcement. The voxel size is $30.05^2 \times 34.00\ \mu m^3$. It is noted that, due to the limitations of the device, there are maximum differences of 0.26 mm (8.7 voxel) between the displacements for the CT scan determined based on the failure point and those where a CT scan was performed.

Fig. 8 shows vertical cross sections of the CT images obtained at 0 mm, 1 mm, 2 mm, 3 mm and 6 mm displacements. In the CT image, the black portions indicate the lower density regions, while the white portions indicate the higher density regions. For Case 1, lower density regions occur upward obliquely at the corner of the rib, and then they develop progressively up to a displacement of 3 mm. The soil density above the rib increases with an increase in the displacement, whereas that around the rib decreases locally. The tendency for the decrease in the soil density around the rib is also observed for Cases 2 and 3. On the other hand, the local decrease in soil density at

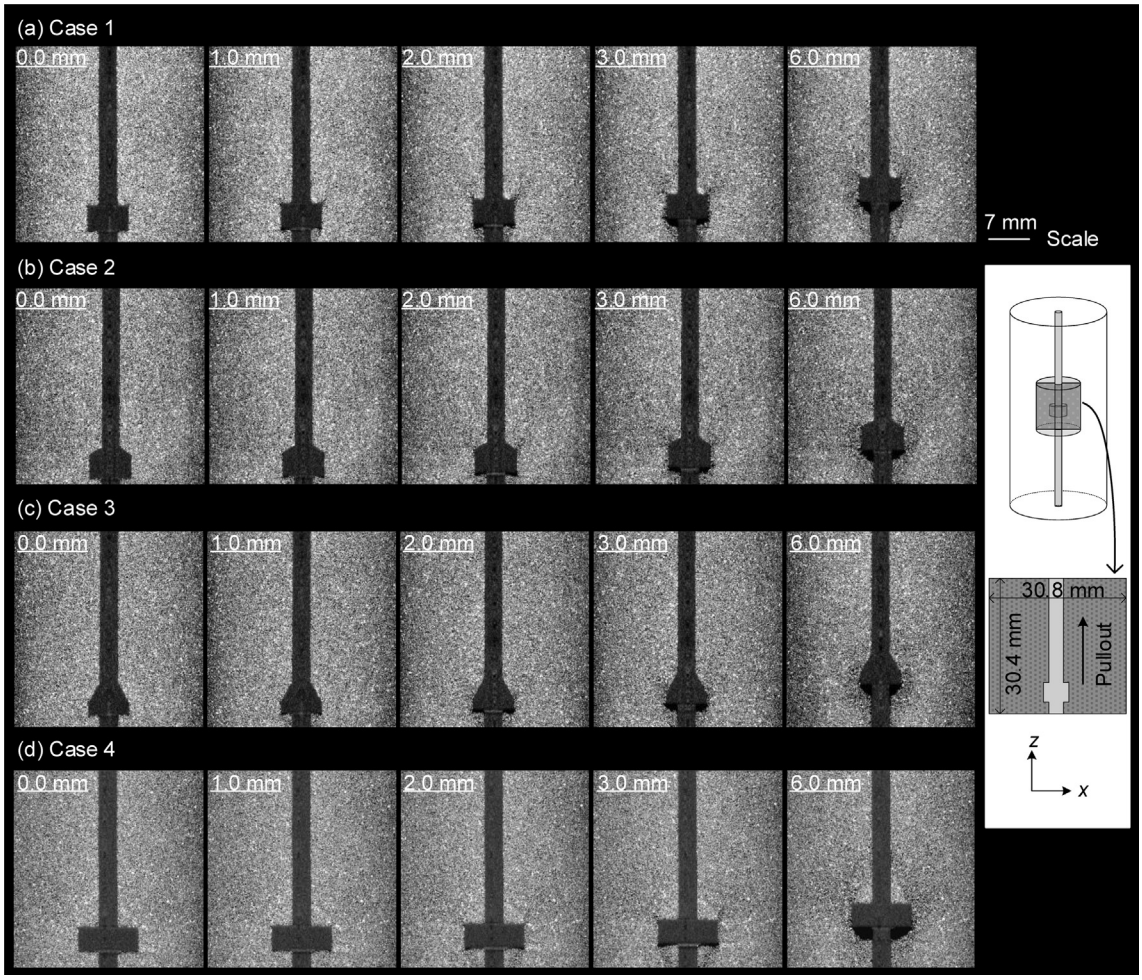

Fig. 8. Vertical cross sections of CT images: (a) Case 1, (b) Case 2, (c) Case 3 and (d) Case 4.

the corner of the rib and the densification of the soil above the rib for Case 1 are more significant than those for Cases 2 and 3.

3.3. Digital image correlation

A digital image correlation (DIC) technique is widely used to measure the deformation process of the target materials using two images of the reference and the deformed states (e.g., Hall et al., 2010; Higo et al., 2013). The three-dimensional displacement fields are obtained by DIC with a zero-normalized cross-correlation coefficient between the reference and the deformed images. The strain levels are calculated by the B matrix for the eight-node isoparametric finite elements. The incremental volumetric strain is defined as a trace of the strain increment tensor, while the second invariant of the incremental deviatoric strain tensor is defined as the shear strain increment. The algorithm of the DIC performed in the present study is described in Higo et al. (2013) in more detail.

The reinforcements used in the present study are axisymmetric, and the soil deformation during the pulling out of the model is assumed to occur symmetrically. Therefore, one quarter of the tomographic volume is chosen as the image analysis region, as shown in Fig. 7. The present study focuses on how soils tend to deform during the pull-out of the reinforcements at given states, rather than where the large soil deformation has cumulated. Such a tendency can be sufficiently observed by incremental displacements calculated from a given pullout displacement level to the next level. It is also confirmed that the tendency for the incremental displacement is qualitatively identical to that for the total displacement calculated from the initial state

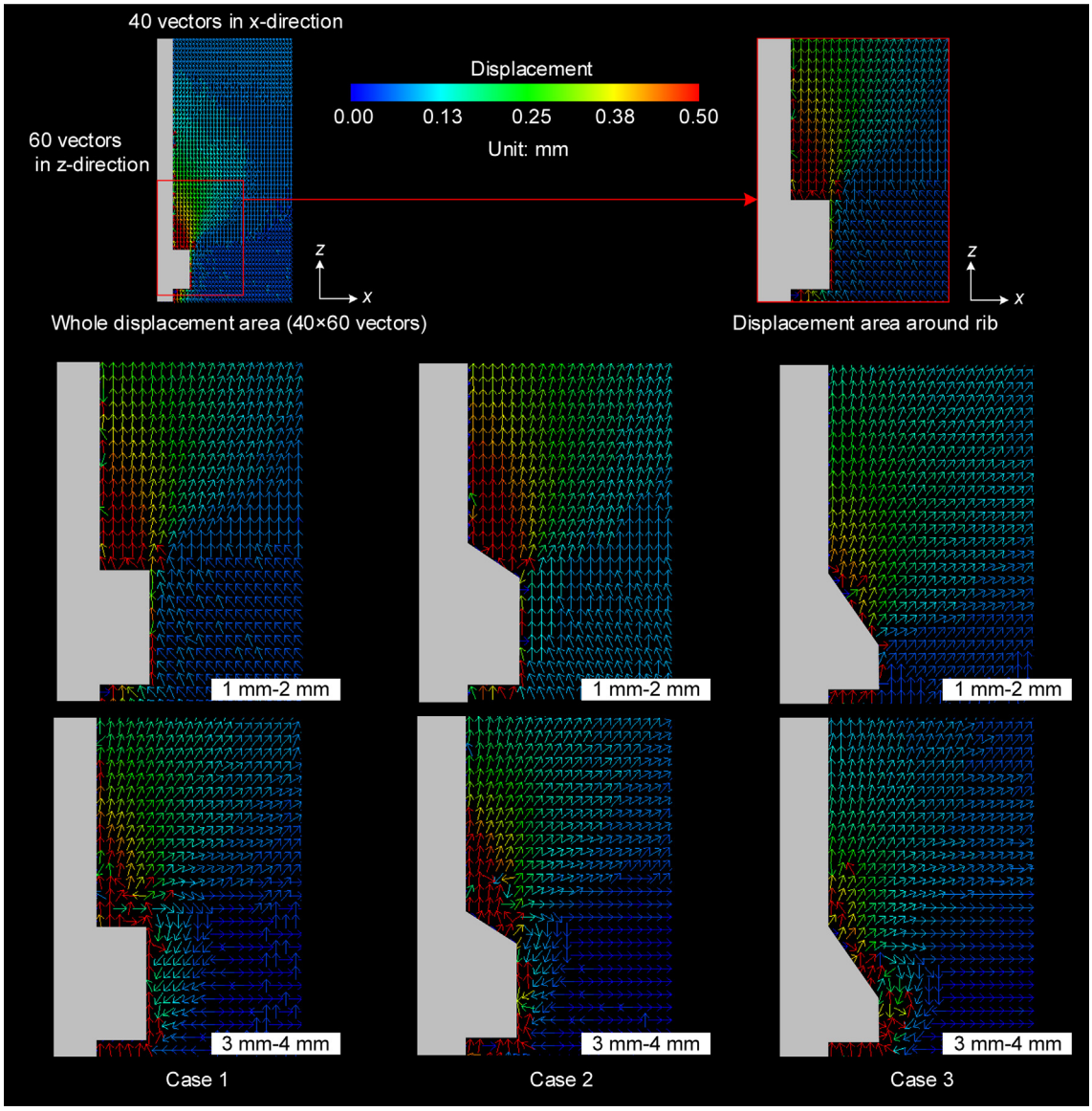

Fig. 9. Distributions of incremental displacement vector around rib.

to a given displacement level. Hence, the soil behaviors are discussed using the incremental displacement.

3.3.1. Incremental displacement vectors

Fig. 9 shows the incremental displacement vectors around the rib for Cases 1 to 3, through which the influence of the rib-inclination angle on the direction in which the soils move around the rib is discussed. The displacement vector in the z-direction corresponds to the soil displacement in the pullout direction (i.e., vertical displacement) and that in the x-direction corresponds to the soil displacement perpendicular to the pullout direction (i.e., horizontal displacement), respectively. CT images at displacements of 1 mm and 2 mm in Fig. 8 and the displacement shown in Fig. 9 are compared. It is found that, for Case 1, relatively large displacements occur above the soil where the density decreases locally around the corner of the rib. For Cases 1 and 2, the soil above the top surface of the rib moves upwards vertically at displacements between 1 mm and 2 mm, whereas the soil also moves upwards to the right and beyond a displacement of 3 mm. At the right side of the rib, the soil above the top surface of the rib moves upwards to the right and the tendency for horizontal soil movements becomes significant with an increase in the displacement. On the other hand, for Case 3, the soil above the rib tends to move upwards to the right even at displacements between 1 mm and 2 mm, as shown in Fig. 9. This is probably because the soil is pushed out in a horizontal direction due to the rearrangement of the soil-particle structures along the top surface of the rib and its tendency is more significant for reinforcements with inclined ribs than those with flat ribs.

A common characteristic for all cases is that the soil at the side of the rib moves downwards to the left at displacements between 3 mm and 4 mm. This is probably because the soil is pushed out and downwards due to the local dilation around the corner of the rib. In a future study, pullout tests using soil particles with a larger diameter will be conducted for measuring microscopic particle kinematics to investigate such a mechanism.

Fig. 10 shows histograms of the soil-displacement angles evaluated for the whole displacement area, i.e., 2400 vectors (40 × 60 vectors in x- and z-directions, respectively), as shown in Fig. 9. The soil-displacement angle is defined as the angle measured from the x-axis to the z-axis. The number of displacement vectors, whose soil-displacement angles are between 0 degrees and 180 degrees, is counted. A bin of the histogram is 5 degrees. At displacements between 1 mm and 2 mm, the histogram for Case 3 is different from those for Cases 1 and 2, while the trend of the histograms among all the cases is almost consistent beyond displacements between 3 mm and 4 mm where the pullout resistance no longer increases. These results confirm that the rib-inclination angle affects the direction in which the soils move until the ultimate pullout resistance is reached, and then its influence becomes small with increasing pullout displacement levels.

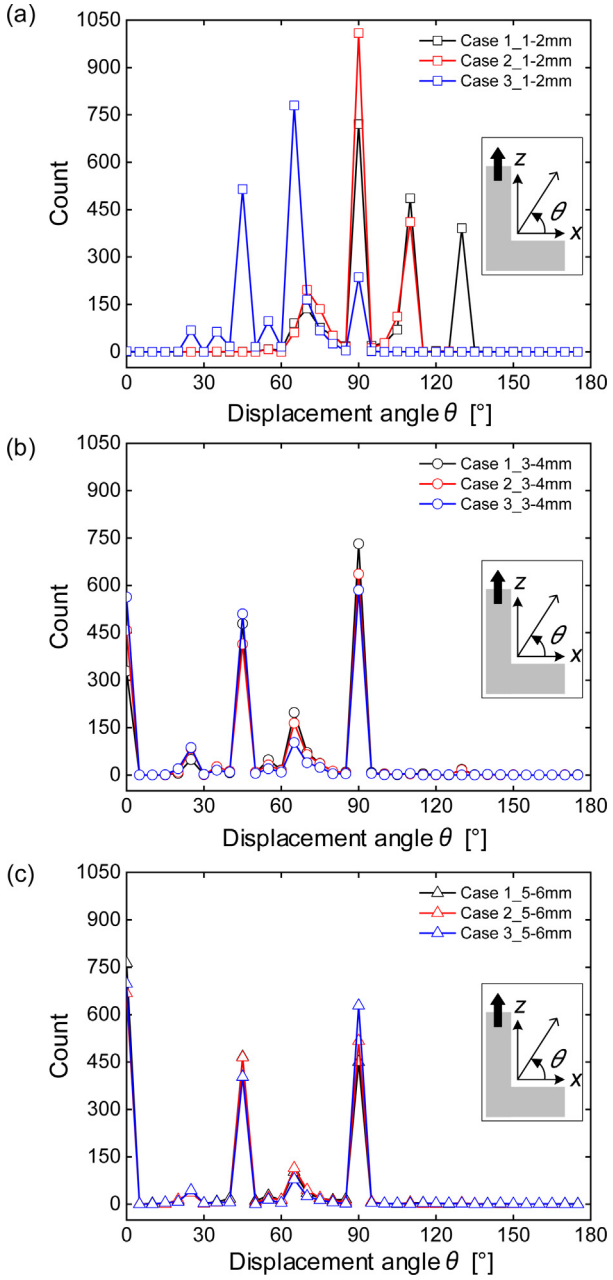

Fig. 10. Distributions of displacement angle at pullout displacement between: (a) 1 mm and 2 mm, (b) 3 mm and 4 mm and (c) 5 mm and 6 mm.

3.3.2. Contour maps of incremental displacement

The tendency for the directions in soil movement is clearly observed in Fig. 9, while the levels of soil movement in horizontal and vertical directions cannot be identified. In this section, the influence of the rib-inclination angle on the levels of vertical and horizontal soil displacements is clarified. Fig. 11 presents contour maps of the whole incremental displacements in each direction. Fig. 12 shows the cumulative vertical and horizontal displacements obtained by integrating the incremental displacement levels over the whole displacement area, as shown in Fig. 9. The plots at a displacement of 2 mm correspond to the results of DIC for displacements between 1 mm and 2 mm. For Case 4, the

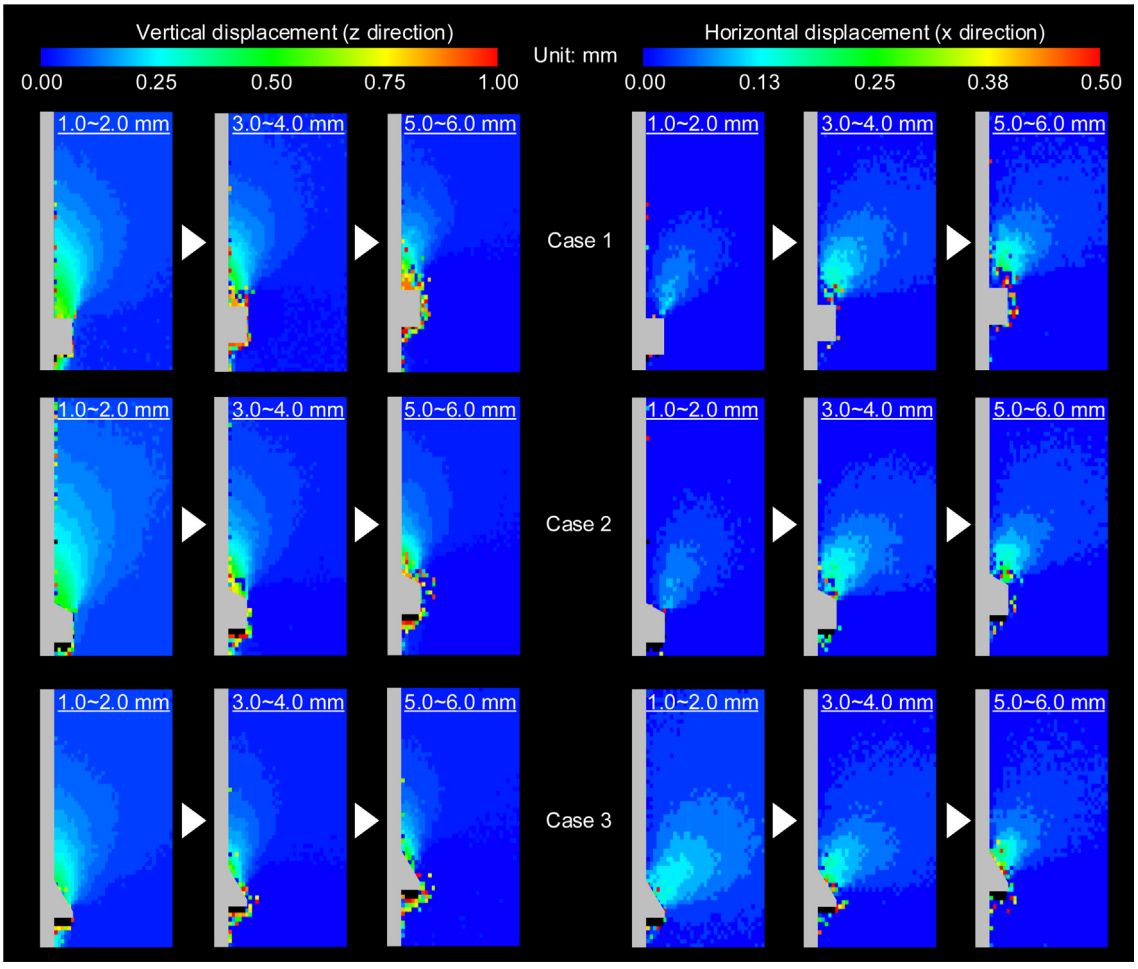

Fig. 11. Contour maps of incremental displacements in vertical and horizontal displacements.

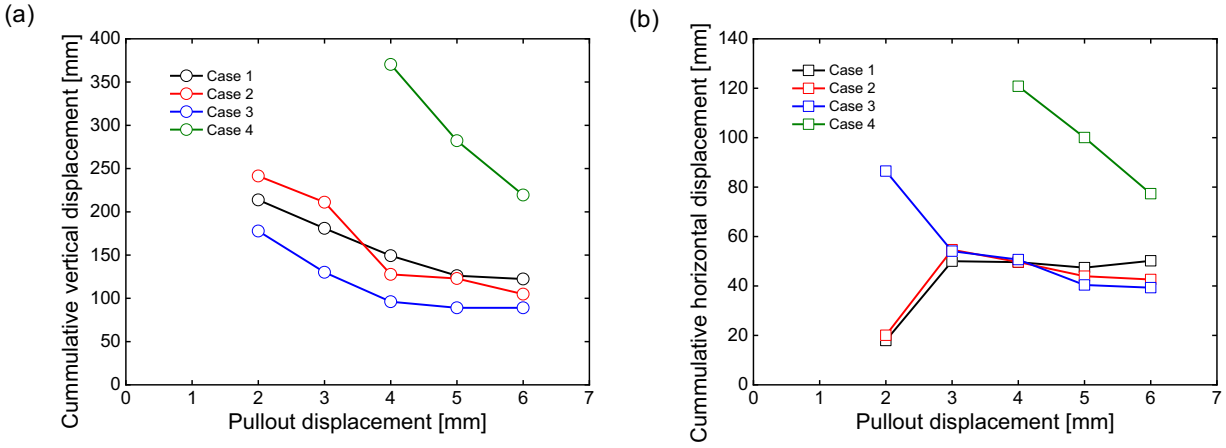

Fig. 12. Cumulative displacement in (a) vertical direction and (b) horizontal direction.

center axis of the reinforcement in the CT images, obtained at displacements of 1 mm and 2 mm, shifts a little from the center axis of the scan area due to a mechanical problem with the CT system, providing inaccurate DIC results. Therefore, the DIC results for Case 4 before the displacement of 3 mm have been omitted from Fig. 12. It is found from this figure that the cumulative displacements in both directions for Case 4 are much larger than those for the other cases. In the following discussion, the results for Cases 1, 2 and 3 are compared.

Firstly, the tendency for the vertical displacement is mentioned. It is clearly seen from Fig. 11 that the level of

vertical displacement is larger at the top surface of the rib for all cases. The area where the vertical displacement occurs gradually radiates at an early state of the pullout, and then it tends to shrink with increasing pullout displacement. In Fig. 12a, the cumulative displacement tends to decrease and it finally converges to almost the same level for all cases with increasing pullout displacement. Although a positive correlation between the vertical displacement and the rib-inclination angle is not clearly observed in the present study, the vertical displacement for Case 3 is smaller than that for Cases 1 and 2 at each pullout displacement.

Next, the tendency for the horizontal displacement is mentioned. It is obvious from Fig. 11 that, at displacements between 1 mm and 2 mm, the horizontal displacement occurs over a wider area for Case 3 than for Cases 1 and 2, while the difference in the displacement area becomes insignificant. It is found from Fig. 12b that transitions in the horizontal displacement for Cases 1 and 2 are almost the same, whereas the horizontal displacement for Case 3 greatly increases at an early stage of the pullout and then converges to a value similar to that for Cases 1 and 2.

It is seen from Fig. 11 that, beyond displacements between 3 mm and 4 mm, the incremental vertical displacement occurs above the rib where the incremental horizontal displacement does not occur, which is more significant in Case 1 than in Case 2. The area corresponds to the higher density region above the rib, as shown in Fig. 8. These results suggest that a rigid soil wedge develops above the rib until the failure state of the soil and follows the movement of the rib.

3.3.3. Distributions of shear strain and volumetric strain

Fig. 13 shows distributions of shear strain and volumetric strain. At displacements between 1 mm and 2 mm, larger shear strain develops locally at the corner of the rib in Cases 1 and 2, while it develops along the rib surface in Case 3. At the same time, the shear strain radiatively develops upwards and occurs at around the shaft of the reinforcement. With an increase in the pullout displacement, the shear strain develops further around the rib for all

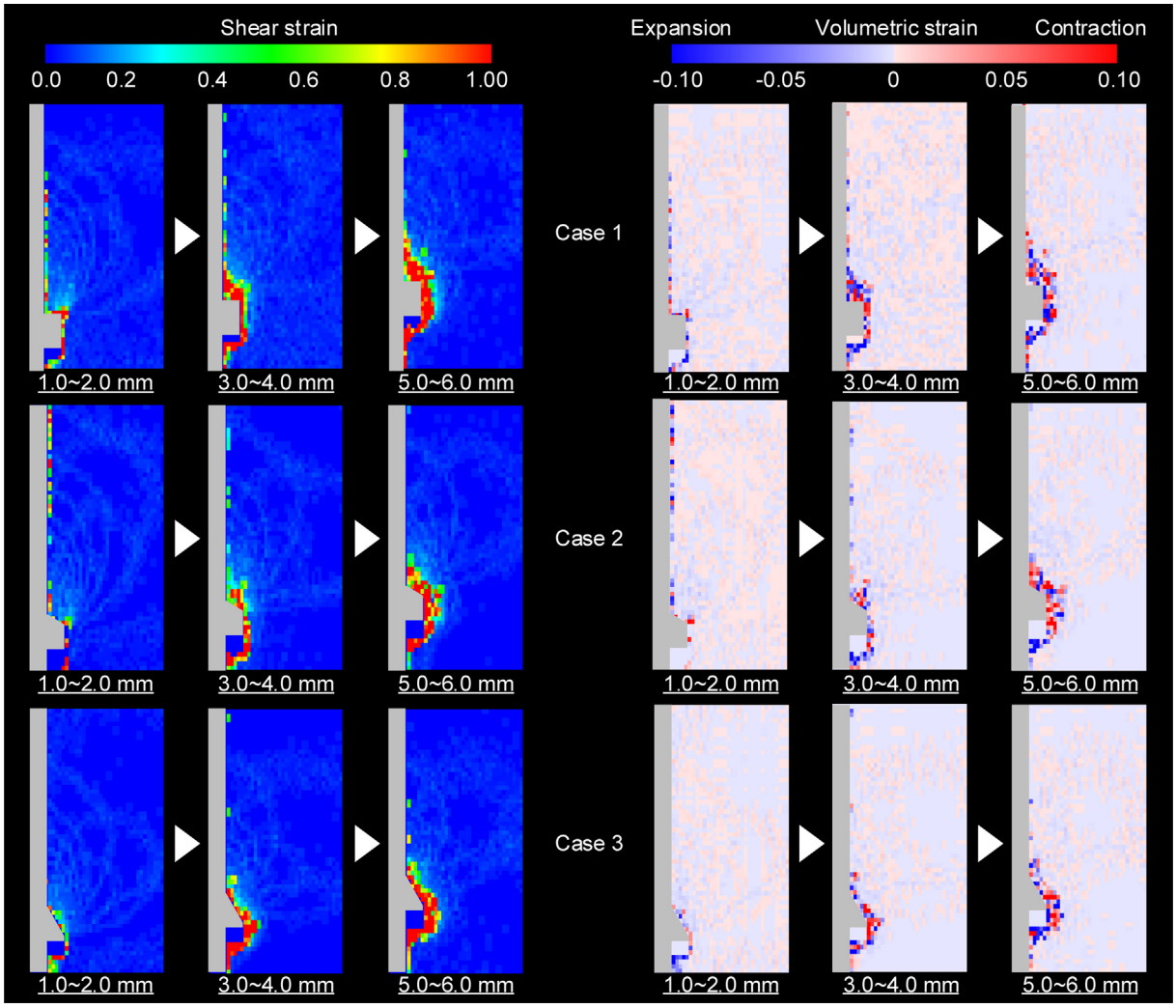

Fig. 13. Distributions of shear strain and volumetric strain.

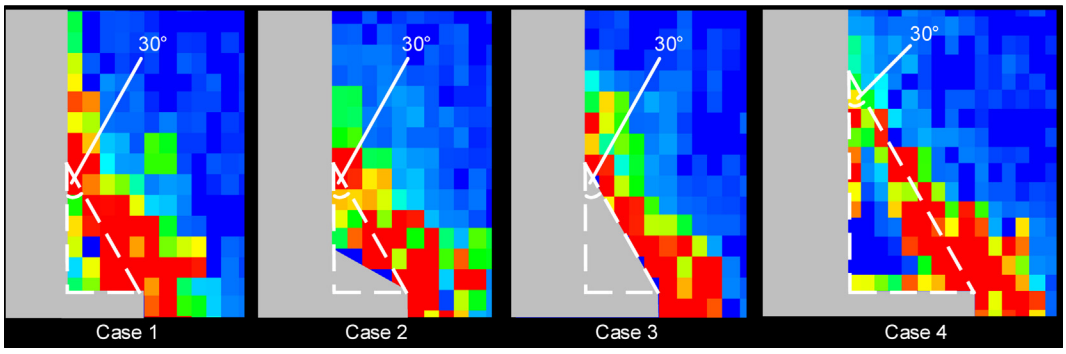

Fig. 14. Comparison of inclination angle of large strain region for Cases 1, 2 and 4 with rib-inclination angle for Case 3.

cases. Therefore, the bearing force above the rib, the shear resistance between the soil particles and the frictional resistance on the surface of the reinforcement contribute to the pullout resistance at an early stage of the pullout, and then the shear resistance between the soil particles around the rib works by increasing the pullout displacement level.

On the other hand, Cases 1 and 2 exhibit different tendencies from Case 3 beyond a pullout displacement of 3 mm, i.e., the failure point. In other words, larger shear strain, indicated in red, occurs upwards to the left from the corner of the rib and shows a gradient with certain degrees for Cases 1 and 2. Fig. 14 presents a comparison of the distributions of shear strain around the rib at pullout displacements between 5 mm and 6 mm for Cases 1 to 4. In this figure, a line with a gradient of 30 degrees, consistent with the rib-inclination angle for Case 3, is described for each case. It is confirmed from this figure that the gradient for Cases 1 and 2 is similar to the rib-inclination angle of 30 degrees for Case 3. Focusing on the distribution of shear strain for Case 4, large shear strain is clearly observed in an oblique direction. No shear strain occurs in the soil above the rib; namely, this region corresponds to the soil wedge which follows the vertical movement of the rib during the pullout. For Cases 1 and 2, certain levels of shear strain occur in the soil just above the rib, but the shear strain developing along the gradient line with 30 degrees is more significant. It is probable, therefore, that the rigid soil wedge developing in Cases 1 and 2 is the same as that in Case 4 and behaves as if it were part of the reinforcements.

Fig. 15 presents a schematic diagram of the similarity in the rib-inclination angles of the reinforcements at the soil-failure state. Here, it is assumed that a vertical rigid wall is pushed to the backfill. It should be noted that, in a strict sense, the soil-deformation characteristics in this situation are a little different from those observed in the present study because there is friction between the soil and the shaft of the reinforcement. The backfill is in a passive failure state with a failure plane inclined at $(\pi/4\text{-}\phi\ /2)$ degrees from the foundation, in which the plastic zone occurs. Assuming that the backfill is composed of Toyoura sand used in the present study, the slope of the passive failure plane is 25.55 degrees when using internal friction angle ϕ^{p} shown in Table 1. This value is similar to the gradient of the large shear strain observed by the DIC and the rib-inclination angle of the reinforcement for Case 3.

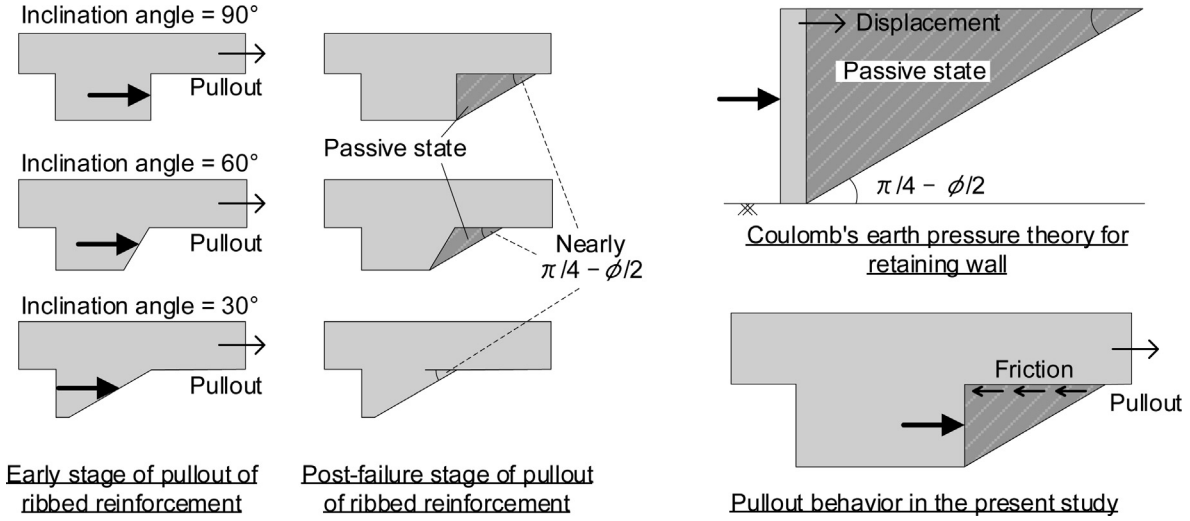

Fig. 15. Schematic illustration of similarity of rib-inclination angle of reinforcements at soil failure state.

Namely, the higher density region, which develops above the rib during the pullout, corresponds to the soil wedge involved with the passive failure. It is certain, therefore, that reinforcements with different degrees of rib-inclination angles come to behave as if they were the same models with increasing pullout displacement.

It is found from Fig. 13 that, for Case 3, both contractive and expansive volumetric strains develop in the soil mainly along the rib surface with increasing pullout displacement. For Cases 1 and 2, the volumetric strains occur in the soil around the corner of the rib at an early stage of the pullout, after which the volumetric strains for the two cases develop in the soil above the rib where the larger shear strain develops. Finally, the distributions of volumetric strain for all cases are almost the same. This is because the movement of the soil particles along the slope of the soil wedge above the rib for Cases 1 and 2 is similar to that along the slope of the rib for Case 3.

3.4. Soil deformation characteristics and their influence on pullout resistance

Fig. 16 shows the relationship between the pullout resistance evolution (explained in Section 3.1) and the soil deformation characteristics (explained in Sections 3.2 and 3.3) during the pullout of reinforcements with different degrees of rib-inclination angles. In the following discussion, for simplicity, the reinforcements for Cases 1 and 2 are referred to as the "large rib-inclination angle model (LIA model)" and that for Case 3 is referred to as the "small rib-inclination angle model (SIA model)". Herein, the soil failure state corresponds to the failure point defined in the present study since the large shear strain around the rib occurs just after the failure point (see Fig. 14), and then soil displacement levels no longer increase in either horizontal or vertical direction (see Fig. 12).

At an early stage of the pullout of a reinforcement (see Stage 1 in Fig. 16), the bearing force above the rib, the shear resistance between soil particles and the frictional resistance on the surface of the reinforcement contribute to the pullout resistance. This mechanism applies to both the SIA and LIA models. On the other hand, the horizontal soil displacement for the LIA model is less significant than that for the SIA model. As a result, the soil densification above the rib is more significant in the LIA model than in the SIA model, contributing to the higher bearing resistance in the LIA model. Therefore, the pullout resistance at an early stage of the pullout of the reinforcement is higher in the LIA model than in the SIA model.

As the soil deformation progresses up to the soil failure state, the rib shape of the LIA model becomes similar to that of the SIA model since the rigid soil wedge related to the passive failure of the soil is generated above the rib. As a result, the influence of the rib-inclination angle on the direction, range and level of the soil displacement becomes small. This characteristic leads to the small difference in the contribution of the bearing resistance to the pullout resistance, although the degrees of the rib-inclination angles of the reinforcements are different from each other. After the soil fails (see Stage 2) in Fig. 16), the shear resistance along the slope of the soil wedge and the rib probably contributes to the pullout resistance rather than the bearing resistance. Soil deformation characteristics, such as the direction, range and levels of the soil displacement, as well as the dilatancy characteristics for the LIA model and the SIA model, are almost the same as each other. Therefore, the pullout resistance for the two models

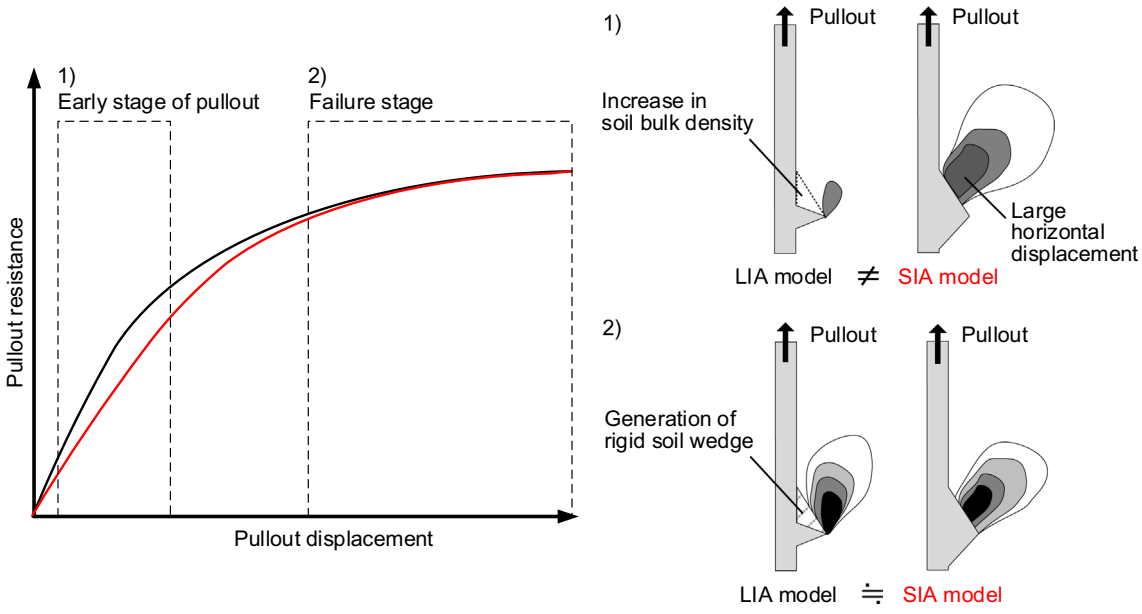

Fig. 16. Relationship between pullout resistance evolution and soil deformation characteristics of reinforcements with different rib-inclination angles.

converges to an equivalent value, even if the degrees of the rib-inclination angles are different from each other.

It is obvious that, under the test conditions in the present study, the rib height exhibits great influence on the pullout resistance rather than the rib-inclination angle. Therefore, the rib-inclination angle (80 degrees for a real model, as shown in Fig. 3a) may be a less significant parameter than the rib height of a ribbed reinforcement (3 mm for a real model, as shown in Fig. 3a) in terms of contributing to the stability of the overall structure. It is certain, however, that the soil dilatancy characteristics depend on the stress levels, which strongly affect the pullout resistance-pullout displacement relationship. It is also assumed that reinforcements experience cyclic push–pull loadings during earthquakes. In this situation, the rib-inclination angle probably affects the pullout resistance evolution. As future works, the soil deformation characteristics during the pullout of reinforcements will be investigated under various levels of confining pressure, cyclic loading conditions. In this case, it may be necessary to prepare the rib inclination on both sides of the reinforcements like real reinforcements, as shown in Fig. 3a. Reinforcements are often placed in the ground at certain inclinations in order to stabilize earth structures (e.g., slopes and cuts). It would be interesting, therefore, to investigate the soil deformation characteristics during the pullout of reinforcements placed in the ground at various inclinations.

4. Conclusions

Pullout tests on ribbed reinforcements and X-ray CT scans were conducted using a triaxial pullout test apparatus developed to clarify the relationship between the soil deformation characteristics and the pullout resistance under isotropic confining pressure. Four models with a rib, i.e., three with different degrees of rib-inclination angles and another one with a larger rib height than the others, were used to investigate the influence of the rib dimensions on the pullout resistance. The displacement and strain fields were calculated using a digital image correlation technique, by which the influence of the rib dimensions on the soil deformation characteristics was revealed. The main findings obtained in the present study are as follows:

1. The soil bulk density above the rib was seen to increase with an increase in the pullout displacement, whereas that around the corner of the rib was seen to decrease. This tendency was found to be more significant for reinforcements with larger rib-inclination angles. The densified region in the soil above the rib brought about the formation of a rigid soil wedge, which is related to the passive failure of the soil, and then the reinforcements with different degrees of the rib-inclination angles came to behave as almost the same models.
2. The soil displacement, perpendicular to the pullout direction, increased greatly at an early stage of the pullout for reinforcements with small rib-inclination angles. On the other hand, such an influence of the rib-inclination angle on the displacement became small as the soil approached the failure state.
3. The rib-inclination angle did not significantly affect the level of the pullout displacement when the pullout resistance no longer increased. On the other hand, larger rib-inclination angles provided higher pullout resistance at an early stage of the pullout. This is because the model with the larger rib-inclination angle exhibited higher bearing resistance related to the densification of the soil above the rib.
4. The pullout resistance of the models with different degrees of the rib-inclination angles tended to converge to a similar level beyond the soil failure state. This is because, for every model, the soil deformation characteristics (e.g., the level and range of the soil displacement, shear strain and volumetric strain) were similar to each other.
5. The rib height of the reinforcement probably affected the pullout resistance more significantly than the rib-inclination angle. This point should be examined by, for example, conducting pullout tests under various levels of confining pressure, cyclic push–pull loading tests and so on.

Acknowledgments

This research was greatly supported by grants given by the Mizuho Foundation for the Promotion of Sciences.

References

Andò, E., Hall, S.A., Viggiani, G., Desrues, J., Bésuelle, P., 2012. Grain-scale experimental investigation of localised deformation in sand: a discrete particle tracking approach. Acta Geotech. 7 (1), 1–13.

Desrues, J., Chambon, R., Mokni, M., Mazerolle, F., 1996. Void ratio evolution inside shear bands in triaxial sand specimens studied by computed tomography. Géotechnique 46 (3), 539–546.

Doreau-Malioche, J., Combe, G., Viggiani, G., Toni, J.B., 2018. Shaft friction changes for cyclically loaded displacement pile: An X-ray investigation. Géotechnique Letters 8 (1), 66–72.

Druckrey, A., Alshibli, K.A., Al-Raoush, R., 2018. Discrete particle translation gradient concept to expose strain localization in sheared granular materials using 3D experimental kinematic measurements. Géotechnique 68 (2), 162–170.

Hall, S.A., Bornert, M., Desrues, J., Pannier, Y., Lenoir, N., Viggiani, G., Bésuelle, P., 2010. Discrete and continuum analysis of localised deformation in sand using X-ray μCT and volumetric digital image correlation. Géotechnique 60 (5), 315–322.

Hamamoto, S., Moldup, P., Kawamoto, K., Sakaki, T., Nishimura, T., Komatsu, T., 2016. Pore network structure linked by X-ray CT to particle characteristics and transport parameters. Soils Found. 56 (4), 676–690.

Higo, Y., Oka, F., Kimoto, S., Sanagawa, T., Matsushima, Y., 2011. Study of strain localization and microstructural changes in partially saturated sand during triaxial tests using microfocus X-ray CT. Soils Found. 51 (1), 95–111.

Higo, Y., Oka, F., Sato, T., Matsushima, Y., Kimoto, S., 2013. Investigation of localized deformation in partially saturated sand under triaxial compression using microfocus X-ray CT with digital image correlation. Soils Found. 53 (2), 181–198.

Higo, Y., Kido, R., Takamura, F., Fukushima, Y., 2018. Pore-scale investigations of partially water-saturated granular soil. Mech. Res. Commun. 94, 1–7.

Hirai, T., Konami, T., Yokata, Y., Utani, Y., Ogata, K., 2003. Case histories of earth reinforcement technique 22 in Japan. In: Proc. the International Symposium on Earth Reinforcement, IS-Kyushu 2003, 23 A.A. Balkema, Fukuoka, Kyushu, Japan, pp. 1009–1020.

James, K.M., Willem, C.B.V., 1987. Reinforcement of earth slopes and embankments. National Cooperative Highway Res. Program report 290.

Jayawickrama, P.W., Lawson, W.D., Wood, T.A., Surles, J.G., 2015. Pullout Resistance Factors for Steel MSE Reinforcements Embedded in Gravelly Backfill. J. Geotech. Geoenviron. Eng. 141 (2), 1–10.

Jones, C.J.F.P., 1985. Earth reinforcement and soil structures. Butterworth's Adv. Series Geotech. Eng.

Kido, R., Higo, Y., 2019. Distribution changes of grain contacts and menisci in shear band during triaxial compression test for unsaturated sand. Japanese Geotech. Soc. Special Publ. 7 (2), 627–635.

Kido, R., Higo, Y., Takamura, F., Morishita, R., Khaddour, G., Salager, S., 2020. Morphological transitions for pore water and pore air during drying and wetting processes in partially saturated sand. Acta Geotech. 15, 1745–1761.

Kikuchi, Y., 2006. Investigation of engineering properties of man-made composite geo-materials with micro-focus X-ray CT. In: Advanced in X-ray tomography for geomaterials, Proc. Second International Workshop on X-ray CT for Geomaterials, GeoX 2006, Aussois, France, pp. 255–261.

Kuwano, J., Miyata, Y., Koseki, J., 2014. Performance of reinforced soil walls during the 2011 Tohoku earthquake. Geosynthetics Int. 21 (3), 1–18.

Lawson, W., Jayawickrama, P., Wood, T., Surles, J., 2013. Pullout Resistance of Mechanically Stabilized Earth Reinforcements in Backfills Typically Used In Texas. TxDOT Research Report, FHWA/TX-13/0-6493-1.

Lee, H.S., Bobet, A., 2005. Laboratory evaluation of pullout capacity of reinforced silty sands in drained and undrained conditions. Geotech. Test. J. 28 (4), 370–379.

Li, L.H., Chen, Y.J., Ferreira, P.M.V., Liu, Y., Xiao, H.L., 2017. Experimental investigations on the pull-out behavior of tire strips reinforced sands. Materials 10 (7).

Miyata, Y., 2014. Reinforced soil walls during recent great earthquakes in japan and geo-risk-based design. In: Maugeri M., Soccodato C. (Eds.), Earthquake Geotechnical Engineering Design. vol. 28. Geotechnical, Geological and Earthquake Engineering, pp. 343–362.

Miura, N., Yamauchi, T., 1977. Effect of particle-crushing on the shear characteristics of a sand. J. Japan Soc. Civil Eng. 260, 109–118 (in Japanese).

Moayedi, H., Mosallanezhad, M., 2017. Uplift resistance of belled and multi-belled piles in loose sand. Measurement 109, 346–353.

Mukunoki, T., Miyata, Y., Mikami, K., Shiota, E., 2016. X-ray CT analysis of pore structure in sand. Solid Earth 7, 929–942.

Ogawa, N., 1997. Frictional characteristics of strips and filling material. J. Japan Soc. Civil Eng. 568, 221–226 (in Japanese).

Otani, J., Mukunoki, T., Obara, Y., 2000. Application of X-ray CT method for characterization of failure in soils. Soils Found. 40 (2), 113–120.

Otani, J., Mukunoki, T., Obara, Y., 2002. Characterization of failure in sand under triaxial compression using an industrial X-ray CT scanner. Int. J. Phys. Modell. Geotech. 1, 15–22.

Otani, J., 2003. State of the art report on geotechnical X-ray CT research at Kumamoto University. In: Proc. of the International Workshop on X-ray CT for Geomaterials, GeoX2003, pp. 43–77.

Public Works Research Center, 2014. Design Method, Construction Manual and Specifications for Steel Strip Reinforced Retaining Walls, 4th revised ed. Public Works Research Center, Tsukuba, Ibaraki, 25 Japan. (in Japanese).

Rahmaninezhad, S.M., Han, J., Weldu, M., Kakrasul, J.I., Razeghi, H.R., 2016. Effects of methods of applying normal stresses in pullout tests on pressure distributions and pullout resistance. In: Proc. of the GeoAmericans 2016, 3rd Pan-American Conference on Geosynthetics, pp. 1308–1315.

Rathje, E.M., Rauch, A.F., Trejo, D., Folliard, K.J., Viyanant, C., Esfellar, M., Ogalla, M., 2006. Evaluation of Crushed Concrete and Recycled Asphalt Pavement as Backfill for Mechanically Stabilized Earth Walls, FHWA/TX-06/0-4177-3.

Richardson, G.N., Feger, D., Fong, A., Lee, K.L., 1977. Seismic testing of reinforced earth walls. J. Geotech. Eng. Division 103 (1), 1–17.

Richardson, G.N., Lee, K.L., 1975. Seismic design of reinforced earth walls. J. Geotech. Eng. Division 101 (2), 167–188.

Sawamatsu, T., Fujita, T., Sato, N., Nitta, T., 2018. Survey of reinforced soil wall damaged by 2016 Kumamoto earthquake. Proc. the 7th China-Japan Geotechnical Symposium, pp. 276–281.

Sawamura, Y., Shibata, T., Kimura, M., 2019. Mechanical role of reinforcement in seismic behavior of steel-strip reinforced earth wall. Soils Found. 59 (3), 710–725.

Schlosser, F., Elias, V., 1978. Friction in reinforced earth. In: Symp. on Earth Reinforcement, ASCE Annual Convention, Pittsburgh, Pennsylvania, USA, pp. 735–763.

Schlosser, F., 1982. Behaviour and design of soil nailing, In: Proc. Of Int. Symp., vol. 29. Held at Asia Institute of Technology, Bankok, pp. 399–419.

Siddharthan, R.V., Ganeshwara, V., Kutter, B.L., El-Desouky, M., Whitman, R.V., 2004. Seismic deformation of bar mat mechanically stabilized earth walls, I: centrifuge tests. J. Geotech. Geoenviron. Eng. 130 (1), 14–25.

Weldu, M., Han, J., Mustapha, S., Rahmaninezhad, S.M., Parsons, R.L., Kakrasul, J.I., Jiang, Y., 2016. Effect of Aggregate uniformity on pullout resistance of steel strip reinforcement. J. Transport. Res. Board 2579, 1–7.